The Astrophysical Journal, 628:1086–1096, 2005 August 1

DISSOCIATIVE CHARGE EXCHANGE AND IONIZATION OF O_2 BY FAST H^+ AND O^+ IONS: ENERGETIC ION INTERACTIONS IN EUROPA'S OXYGEN ATMOSPHERE AND NEUTRAL TORUS

H. Luna,[1] C. McGrath,[1] M. B. Shah,[1] R. E. Johnson,[2] M. Liu,[2]
C. J. Latimer,[1,3] and E. C. Montenegro[4]

Received 2004 November 16; accepted 2005 March 23

ABSTRACT

Measurements of electron capture and ionization of O_2 molecules in collisions with H^+ and O^+ ions have been made over an energy range 10–100 keV. Cross sections for dissociative and nondissociative interactions have been separately determined using coincidence techniques. Nondissociative channels leading to O_2^+ product formation are shown to be dominant for both the H^+ and the O^+ projectiles in the capture collisions and only for the H^+ projectiles in the ionization collisions. Dissociative channels are dominant for ionizing collisions involving O^+ projectiles. The energy distributions of the O^+ fragment products from collisions involving H^+ and O^+ have also been measured for the first time using time-of-flight methods, and the results are compared with those from other related studies. These measurements have been used to describe the interaction of the energetic ions trapped in Jupiter's magnetosphere with the very thin oxygen atmosphere of the icy satellite Europa. It is shown that the ionization of oxygen molecules is dominated by charge exchange plus ion impact ionization processes rather than photoionization. In addition, dissociation is predominately induced through excitation of electrons into high-lying repulsive energy states (electronically) rather than arising from momentum transfer from knock-on collisions between colliding nuclei, which are the only processes included in current models. Future modeling will need to include both these processes.

Subject headings: atomic processes — molecular processes — planets and satellites: individual (Europa, Jupiter)

1. INTRODUCTION

Dissociation of molecular oxygen by energetic ions remains a relatively little studied area, despite the role that such collisions can play in atmospheric chemistry. Of recent interest are the thin oxygen-rich atmospheres of Jupiter's icy moons Europa and Ganymede. These atmospheres are produced by interactions of energetic charged particles with the moons' icy surfaces in which processes that give rise to chemical changes occur (Johnson et al. 2003, 2004). These processes, called radiolysis, are limited by interactions with the energetic ions trapped in Jupiter's magnetosphere (Saur et al. 1998; McGrath et al. 2004). The energetic component of the incident ions is predominantly protons, oxygen, and sulfur ions (Cooper et al. 2001; Paranicas et al. 2002). Collisions with these ions can lead to the formation of energetic neutrals by charge exchange and, as we show, the production of substantial amounts of charged and neutral fragments. As molecular binding energy becomes converted into kinetic energy of O_2 fragments, dissociated fragments can have sufficient energy to cause them to escape from the gravitational field of these moons. Those neutrals that escape from Europa's oxygen atmosphere form an extended cloud of gas gravitationally bound to Jupiter but orbiting with Europa (Schreier et al. 1993; Burger & Johnson 2004). If the neutral species are long lived, they produce a toroidal neutral cloud about the satellite's orbit. The hydrogen component of this gas was recently imaged by an instrument on *Cassini* by the detection of the energetic ($\gtrsim$10 keV) neutrals produced in charge exchange collisions (Mauk et al. 2003), and the smaller oxygen component was directly observed by the UV instrument (Hansen et al. 2003). An instrument to image the very thin atmospheres of the icy Galilean satellites using energetic neutrals produced from charge exchange will likely be included on the proposed *Jupiter Icy Moon Orbiter*.

In the Jovian magnetosphere the new ions produced in the charge exchange and ionization collisions are also "picked up" and accelerated in Jupiter's rotating magnetosphere, heating and populating the plasma. These ions can in turn impact the satellite surfaces and atmospheres, resulting in an interesting feedback process. Therefore, the collision processes studied here can affect the total energy balance and loss rates of the icy satellite atmospheres, the production and heating of the Jovian magnetospheric plasma, and the detection of atmospheric O_2.

Oxygen produced by radiolysis and photolysis (interactions involving photons) of the surfaces of Saturn's icy moons and ring particles will contribute to the giant toroidal atmosphere in Saturn's magnetosphere (Jurac et al. 2002). Molecular oxygen ions were seen over the rings and in the inner magnetosphere on *Cassini*'s first pass through Saturn's magnetosphere (Young et al. 2005), confirming the presence of molecular oxygen in Saturn's magnetosphere. Charge exchange between these molecules and the energetic ions trapped in Saturn's magnetosphere, the process studied here, leads to the production of energetic neutrals. These can be detected by *Cassini* (Krimigis et al. 2005) and used to study the oxygen density in Saturn's magnetosphere.

We report here cross sections for capture and ionizing collisions by H^+ and O^+ incident on O_2 over an energy range 10–100 keV, a range of considerable relevance at the icy moons of Jupiter and Saturn. The most pronounced reaction channels within this energy range have been considered. The channels

[1] Department of Pure and Applied Physics, Queen's University Belfast, Belfast BT7 1NN, UK.
[2] Department of Engineering Physics, University of Virginia, Charlottsville, VA 22904.
[3] Corresponding author: c.latimer@qub.ac.uk.
[4] Departamento de Física, Universidade Pontificia Universidade Catolica do Rio de Janeiro, Caixa Postal 38071, Rio de Janeiro 22452-970, Brazil.

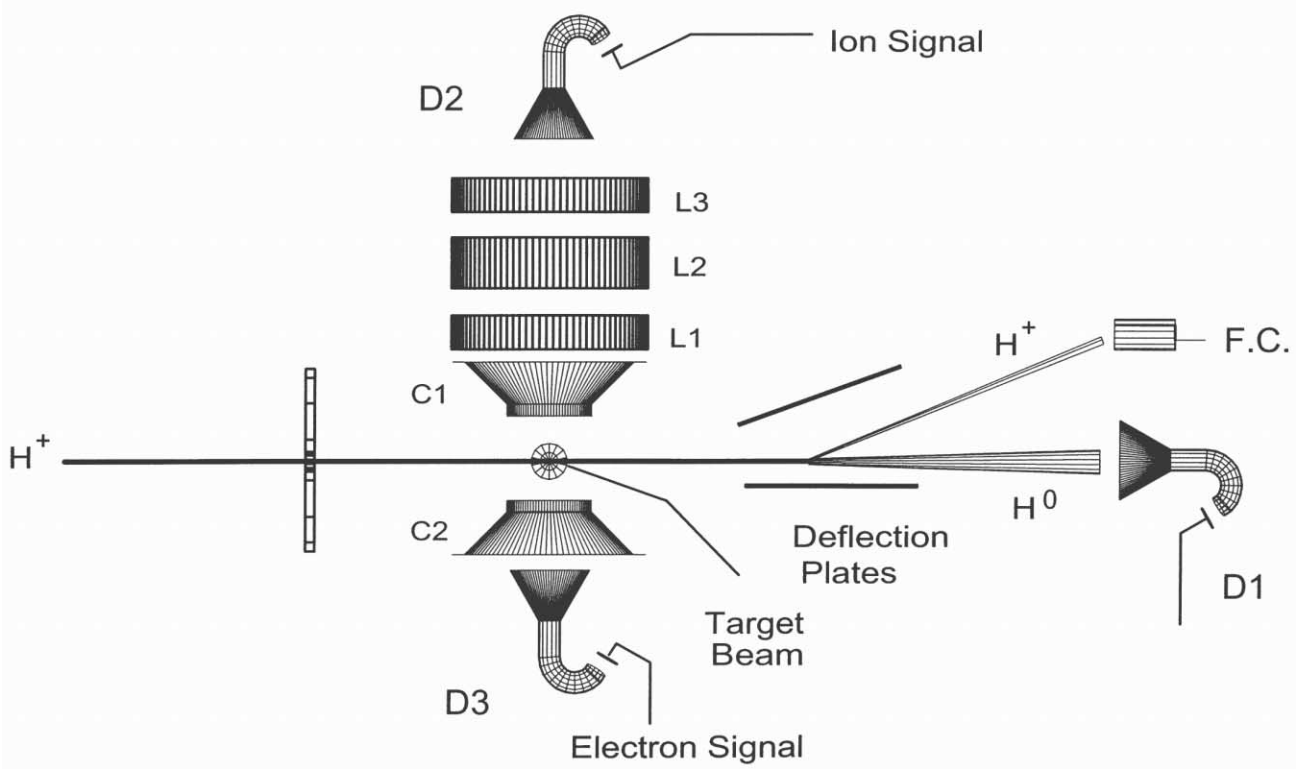

FIG. 1.—Schematic diagram of the apparatus. C1 and C2 are a pair of cylindrical extraction electrodes surrounding the interaction region at right angles to the projectile and the target beams. L1, L2, and L3 are the elements of an electrostatic lens system. D1, D2, and D3 are the particle detectors, and the Faraday cup (F. C.) is used to monitor the intensity of the projectile ion beam.

resulting in the production of fast H or O neutrals are (with an H^+ projectile used for illustration)

$$H^+ + O_2 \rightarrow H + O_2^+ \quad (1)$$

for the nondissociative electron capture collisions leading to O_2^+ formation,

$$H^+ + O_2 \rightarrow H + O^+ + O \quad (2)$$

for the dissociative electron capture collisions leading to $O^+ + O$ formation,

$$H^+ + O_2 \rightarrow H + O^+ + O^+ + e \quad (3)$$

for the dissociative transfer ionization (TI) collisions leading to $O^+ + O^+$ pair formation, and the capture collisions

$$H^+ + O_2 \rightarrow H + O^{++} + O + e \quad (4)$$

leading to O^{++} formation.

The following ionization cross sections in which the projectile charge remains unchanged have also been measured:

$$H^+ + O_2 \rightarrow H^+ + O_2^+ + e \quad (5)$$

for the nondissociative collision channel leading to O_2^+ formation,

$$\begin{aligned} H^+ + O_2 &\rightarrow H^+ + O^+ + O + e \\ &\rightarrow H^+ + O^+ + O^+ + 2e \end{aligned} \quad (6)$$

for the dissociative collision channel leading to $O^+ + O$ and $O^+ + O^+$ pair formation, and

$$H^+ + O_2 \rightarrow H^+ + O^{++} + O + 2e \quad (7)$$

for the dissociative collision channel leading to O^{++} formation.

It should be noted that in the case of O^+ incident ions, further channels involving multiple electron loss from the projectile are possible. However, these are known (Jorgensen et al. 1965) to be over an order of magnitude smaller than processes in which the O^+ projectiles loose no electrons or capture one electron, and so have not been considered in the present investigation. The laboratory results are first presented and discussed. These are then applied to the interaction of H^+ and O^+ with Europa's oxygen atmosphere and its extended neutral cloud.

2. EXPERIMENTAL APPROACH

The main apparatus and experimental procedure have been described previously (Luna et al. 2003; McCartney et al. 1999; McGrath et al. 2001), and only the main features and minor modification need be summarized here. Figure 1 shows the schematic diagram of the apparatus used. A pulsed beam of H^+ or O^+ ions was crossed at 90° by a well-collimated thermal energy beam of O_2. Slow target product ions and electrons were extracted in opposite directions from the interaction region and detected using channel electron multipliers D2 and D3, and identified by time of flight (TOF). The reaction channels (1) and (4) were identified by recording the target products in coincidence with fast neutral products detected by D1, as was the sum of channels (2) and (3). Channel (3) was uniquely determined by triple coincidences involving detectors D1, D2, and D3. The ionization channels (5), (6), and (7) were identified by

TABLE 1

Cross Sections for the Dissociative and Nondissociative Capture and Ionization Channels for H^+ Ion Impact on O_2

E (keV)	Channel Number						
	(1)	(2)	(3)	(4)	(5)	(6)	(7)
10	55.8 ± 4.4	14.0 ± 1.8	5.1 ± 0.6	0.27 ± 0.02	8.5 ± 1.1	9.4 ± 1.2	0.36 ± 0.07
20	39.9 ± 3.2	16.9 ± 2.2	7.1 ± 0.9	0.64 ± 0.05	15.0 ± 1.9	14.3 ± 1.8	0.79 ± 0.10
30	25.6 ± 2.0	12.6 ± 1.6	6.1 ± 0.8	0.72 ± 0.06	21.5 ± 2.8	19.9 ± 2.6	1.40 ± 0.18
40	23.6 ± 1.9	14.9 ± 1.9	6.8 ± 0.9	0.97 ± 0.08	23.8 ± 3.1	18.7 ± 2.4	1.40 ± 0.18
50	18.6 ± 1.5	13.1 ± 1.7	6.3 ± 0.8	0.97 ± 0.08	25.7 ± 3.3	19.7 ± 2.6	1.67 ± 0.22
60	13.9 ± 1.1	10.2 ± 1.3	6.1 ± 0.8	0.97 ± 0.08	29.7 ± 3.8	21.4 ± 2.7	1.66 ± 0.21
70	10.9 ± 0.9	8.5 ± 1.1	5.1 ± 0.7	0.89 ± 0.07	29.9 ± 3.9	20.4 ± 2.7	1.58 ± 0.19
80	8.9 ± 0.7	7.2 ± 0.9	4.2 ± 0.6	0.76 ± 0.06	30.5 ± 3.9	20.9 ± 2.7	1.60 ± 0.21
90	7.1 ± 0.5	6.2 ± 0.8	3.6 ± 0.5	0.63 ± 0.05	29.6 ± 3.8	19.9 ± 2.6	1.56 ± 0.20
100	5.7 ± 0.4	4.9 ± 0.6	3.0 ± 0.4	0.53 ± 0.04	29.3 ± 3.8	19.2 ± 2.5	1.37 ± 0.18

Notes.—Units for channels (1)–(7) are 10^{-17} cm^2. Errors represent 1 standard deviation.

recording the coincidences between the target products and the emitted electrons. The present cross sections have been normalized to the well-established total one-electron-capture cross sections of Stier & Barnett (1956) for proton impact. These cross sections corresponding to the sum of the channels (1), (2), (3), and (4) are believed to be accurate to within 5%. It should be noted that channel (4) involves the production of electrons and so can be used to calibrate the electron detector D3, thus also permitting the normalization of channels (5), (6), and (7) to the Stier & Barnett data (for full details, see Luna et al. 2003).

Fragment ion energy distribution measurements were made without the application of an extraction voltage across the interaction region. As a result, ions proceeded to the detector D2 in the absence of any external field that might cause changes to their velocity. A reference pulse obtained from the main projectile beam pulser was used as a start pulse to produce TOF spectra. Fragment ion energy distributions arising from Coulomb explosions, which involve the production of O^+-O^+ ion pairs, required an additional signal from the second O^+ ion. This was obtained from the detector D3. The measured TOF spectra were converted into energy spectra using standard procedures (Auerbach 1988).

Ion sources of the type used in this study are known to produce, in addition to $O^+(^4S)$ ground-state ions, a substantial fraction (~20%) of $O^+(^2D)$ and $O^+(^2P)$ metastable ions (Stebbings et al. 1966). The results presented here therefore pertain to an unknown mixture of oxygen ion states. However, it should be noted that, at the relatively high collision energies employed in the present work, it is now well established that charge transfer cross sections for both ground-state and metastable oxygen ions are identical (Lindsay et al. 1998).

3. RESULTS AND DISCUSSION

3.1. *Electron Capture and Ionization Cross Sections*

Our measured cross sections for the channels (1)–(7) are tabulated in Tables 1 and 2 for incident H^+ and O^+ ions, respectively, over the energy range 10–100 keV. The individual error bars (1 standard deviation) given in the tables include contributions from statistical uncertainties in the accumulated counts, uncertainties in the reproducibility of the measurements, uncertainties in the calibration of the detectors, and, where appropriate, errors involved in subtraction procedures adopted to extract data for the individual channels (for further details, see Luna et al. 2003). The cross sections are subject to a further uncertainty of 8% for channels (1)–(4) and 13% for the remainder, resulting from normalizing uncertainties associated with assigning absolute values for our cross sections to the H^+ impact one-electron-capture cross sections of Stier & Barnett (1956; see Luna et al. 2003). The individual cross sections are shown in Figure 2. For clarity, the capture channels are shown in the top panels and the ionization channels in the bottom panels of the figure. It should be noted that O^+ and O_2^{++} ions have identical charge-to-mass ratios and cannot be distinguished from each

TABLE 2

Cross Sections for the Dissociative and Nondissociative Capture and Ionization Channels for O^+ Ion Impact on O_2

E (keV)	Channel Number						
	(1)	(2)	(3)	(4)	(5)	(6)	(7)
10	134 ± 10	47.8 ± 6.2	5.3 ± 0.7	0.21 ± 0.02	9.6 ± 1.3	31.2 ± 4.1	3.4 ± 0.4
20	158 ± 12	55.3 ± 7.1	7.9 ± 1.0	0.8 ± 0.1	9.6 ± 1.3	42.5 ± 5.5	4.9 ± 0.6
30	148 ± 12	58.1 ± 7.5	9.3 ± 1.2	1.4 ± 0.1	9.5 ± 1.2	48.4 ± 6.3	6.7 ± 0.9
40	153 ± 12	58.2 ± 7.5	11.6 ± 1.5	2.0 ± 0.2	9.4 ± 1.2	52.6 ± 6.8	8.8 ± 1.1
50	146 ± 12	60.1 ± 7.8	12.7 ± 1.6	2.5 ± 0.2	9.6 ± 1.2	54.1 ± 7.0	11.3 ± 1.5
60	141 ± 11	64.1 ± 8.3	13.3 ± 1.7	2.8 ± 0.2	9.2 ± 1.2	52.1 ± 6.8	12.1 ± 1.6
70	132 ± 11	64.9 ± 8.3	15.1 ± 2.0	3.7 ± 0.3	9.8 ± 1.3	56.0 ± 7.3	14.1 ± 1.8
80	127 ± 10	64.9 ± 8.4	15.2 ± 2.0	4.1 ± 0.3	9.4 ± 1.2	56.9 ± 7.4	15.5 ± 2.0
90	114 ± 9	64.1 ± 8.4	16.2 ± 2.0	4.3 ± 0.3	10.3 ± 1.3	57.2 ± 7.4	17.5 ± 2.3
100	104 ± 8	60.5 ± 7.8	15.6 ± 2.0	4.8 ± 0.4	10.3 ± 1.3	54.1 ± 7.0	17.6 ± 2.3

Note.—Units for channels (1)–(7) are 10^{-17} cm^2.

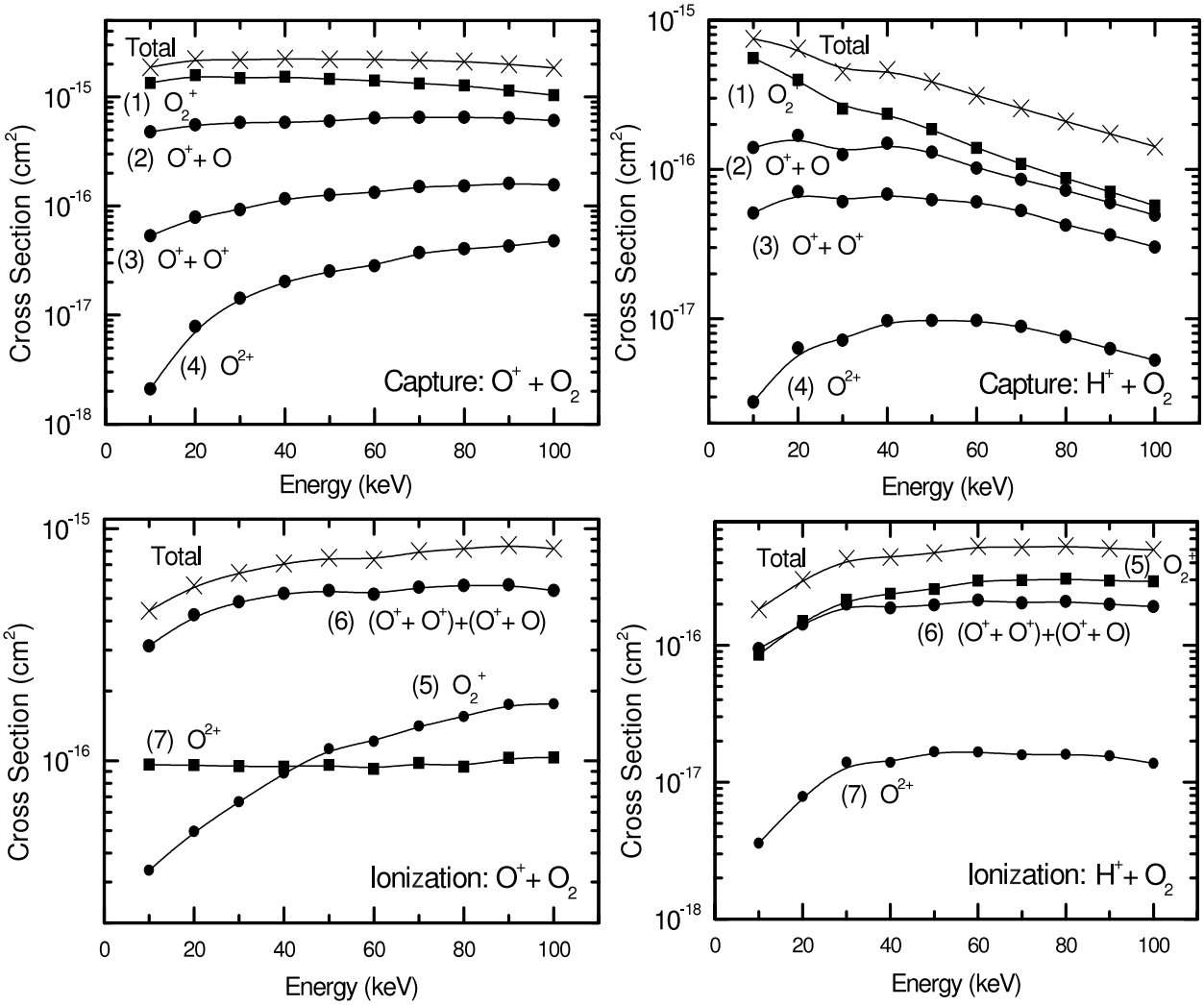

FIG. 2.—Dissociative and nondissociative cross sections for channels (1)–(7) in collisions with H^+ and O^+ ions (see text). Capture cross sections are shown in the top panels, and ionization cross sections in the bottom panels. Total cross sections for the capture channels and the ionization channels are also included for completeness. Error bars are too small to show.

other. However, previous work involving the CO molecule, in which the fragmentation pattern is similar to that observed for the O_2 molecule, has found that the cross sections for forming doubly charged molecular ions in both the electron capture and ionization processes are approximately 2 orders of magnitude smaller at these velocities (Afrosimov et al. 1974). Thus, the error in neglecting the doubly charged species in the present work can be considered negligible.

It is apparent from Figure 2 that the nondissociative capture channel (1) is the largest for H^+ and O^+ incident ions. For ionization, the nondissociative ionization channel (5) is also the largest for H^+. However, the dissociative channels (2), (3), and (6) make significant contributions to the total cross sections in all the three cases. For O^+ impact, the dissociation channel (6) completely dominates the ionization. Dissociation of O_2 is thus a highly probable occurrence for collisions involving H^+ and O^+ projectiles within the present energy range and possibly at higher energies, judging by the trends shown by our high-energy cross sections. For H^+ incident ions, the dissociative channels contribute around 25% and 60% to the total capture cross sections at the energies of 10 and 100 keV, respectively, and almost a constant 50% over the whole energy range to the total ionization cross sections. For O^+ incident ions, the total capture cross sections receive 28% and 43% from the dissociative channels at 10 and 100 keV energies, respectively, and 78% and 87%, respectively, go to the total ionization cross sections. The production of O^{++} product ions created from O_2 targets is not insignificant. At 100 keV, O^{++} production is almost 4% of the total capture for H^+ and 2% for O^+ incident ions. For ionization, it is just over 2% of the total for H^+ over the whole energy range, and for O^+ incident ions it is about 8% at 10 keV and 22% at 100 keV.

There are interesting differences in cross sections between the H^+ and the O^+ incident ions. For instance, the cross sections for the capture channels fall rapidly with increasing energy for H^+ but remain almost constant for O^+. Noting that 100 keV O^+ and 6.25 keV H^+ ions have the same velocity, it can be seen that the equivelocity cross sections for the two projectiles show a reasonable accord for the largest reaction channel (1). However, the dissociative capture channels (2), (3), and (4), which require the transfer of large amounts of excitation energy, show no such accord. For ionization, the differences between the two projectiles become even more interesting. For the O^+ projectile the dissociative channel (6) is the largest, and channel (7), which gives rise to O^{++} ions, is also significantly large, becoming larger than channel (5) at higher energies. For H^+ projectiles, channels (5) and (6) are comparable over all the present range, with channel (7) remaining over an order of magnitude smaller.

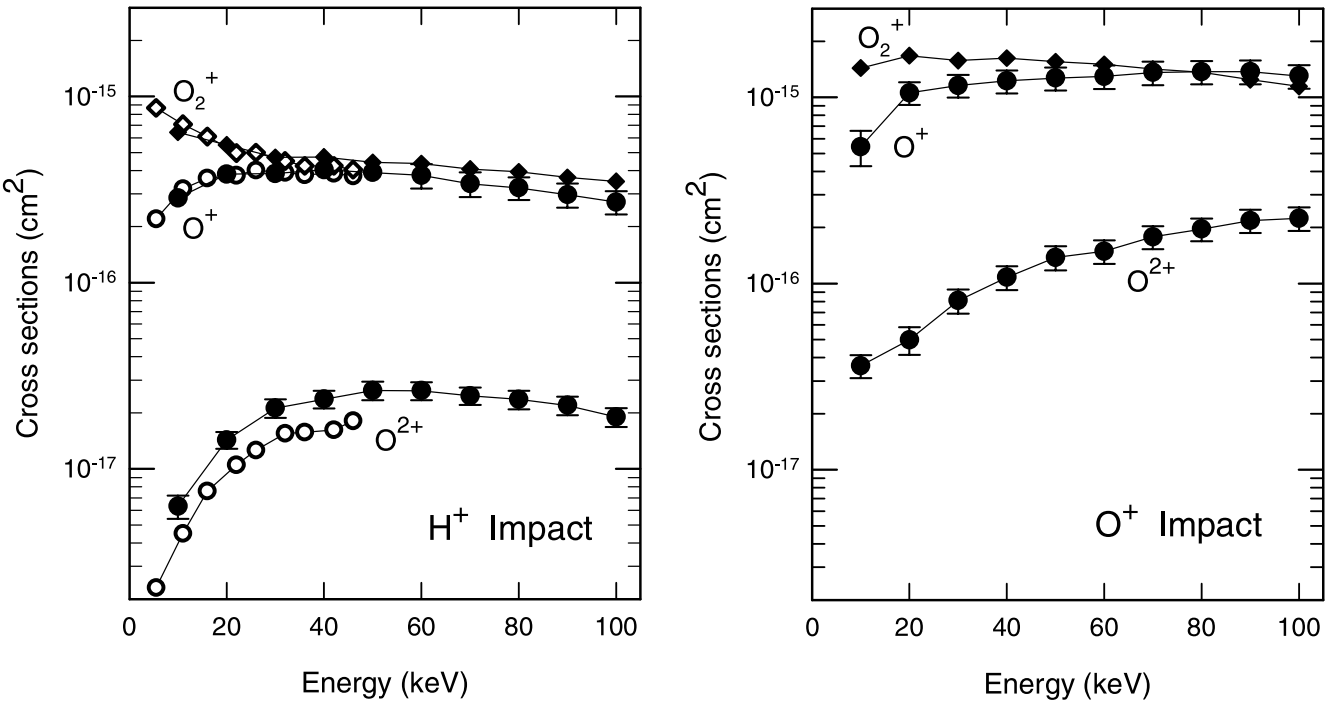

FIG. 3.—Total cross sections for production of O_2^+, O^+, and O^{++} ions in collisions of H^+ and O^+ ions with O_2. *Filled symbols*, present data; *open symbols,* Browning & Gilbody (1968). Error bars are shown when larger than the data points. Quoted errors for the Browning & Gilbody data are 5%.

The different behavior with O^+ could be explained if one considers that these ions move much more slowly than the H^+ ions and thus undergo longer interaction times. This, along with the large kinetic energies that they bring to the collision, means that they would have little difficulty providing the large excitation energies needed in reactions involving channels (6) and (7).

Previous cross sections where the O_2 target products have been recorded separately are available for the H^+ impact only. Browning & Gilbody (1968) measured total cross sections for the O_2^+, O^+, and O^{++} formation from both the capture and the ionization collisions. They are compared with our capture and ionization summed cross sections for the production of O_2^+, O^+, and O^{++} ions in Figure 3 (*left*). It is seen that the agreement is excellent for the total production of the O_2^+ ions and the O^+ ions both in magnitude and in the shape of their energy dependence. Although qualitatively similar, agreement is not so good for O^{++} product ions, where the two sets of data differ by almost a factor of 2. For completeness, we also include similar summed cross sections for O^+ incident ions in Figure 3 (*right*). It is clear that dissociative collisions are as important as the nondissociative collisions, and indeed for O^+ projectiles dissociative processes become comparable to nondissociative processes at high collision energies.

3.2. *Fragment Ion Energy Spectra*

In Figure 4 we show our measured kinetic energy release (KER) energy spectra for H^+ and O^+ projectiles at the incident energies of 20 and 100 keV. Because the target is a homonuclear diatomic molecule, the energy spectra also apply to neutral O fragments. In these measurements, contributions from the capture and the ionization channels could not be separated with any degree of confidence, and so the curves marked O^+ include contributions from channels (2), (3), and (6), and the curves marked $O^+ + O^+$ include contributions from channels (3) and (6). Nor was it possible to separate contributions of the O^{++} ions from the O^+ ions. However, as noted above, O^{++} production is around a few percent, and it is thus safe to assume that our measured energy distribution spectra arise entirely from O^+ contributions. The high-energy component of our distribution for the total O^+ production is entirely dominated by contributions from the Coulomb repulsive states leading to $O^+ + O^+$ production. They account for almost half of the O^+ total for H^+ and O^+ incident ions at 100 keV, and although their contribution is considerably reduced at 20 keV, they still remain significant even for the slowly moving O^+ ions. Once the $O^+ + O^+$ component is subtracted from the O^+ total, it is clear that the remainder $O^+ + O$ component contributes exclusively to the low-energy portion of the energy distribution.

In Figure 5 we show the $O^+ + O^+$ and the $O^+ + O$ components for the 100 keV H^+ ions. As seen, the $O^+ + O$ spectra exhibit a number of well-defined peaks at the low-energy end and a number of intermingled broad peaks at higher energies. This is in close agreement with previous measurements of Yousif et al. (1987) involving He^+ incident ions over the 3–25 keV energy range. In our measurements we used long accumulation times to reduce fluctuations of counting statistics to a negligible amount, and consequently the very sharp noiselike peaks seen in the energy distributions of Figures 4 and 5 are genuine and can be attributed to the presence of vibrational states. Although our present energy resolution was unable to resolve these features fully, it is worth pointing out that we could have increased our energy resolution considerably if we had used a larger separation distance between the ion detector and the interaction region. However, in the present work we are interested in modeling the collision processes that occur on Europa. This requires total cross sections, and so the complete collection of all the target products was of utmost importance, implying the need to use as short a distance as possible. The present distance of 40 mm was found to be the best compromise.

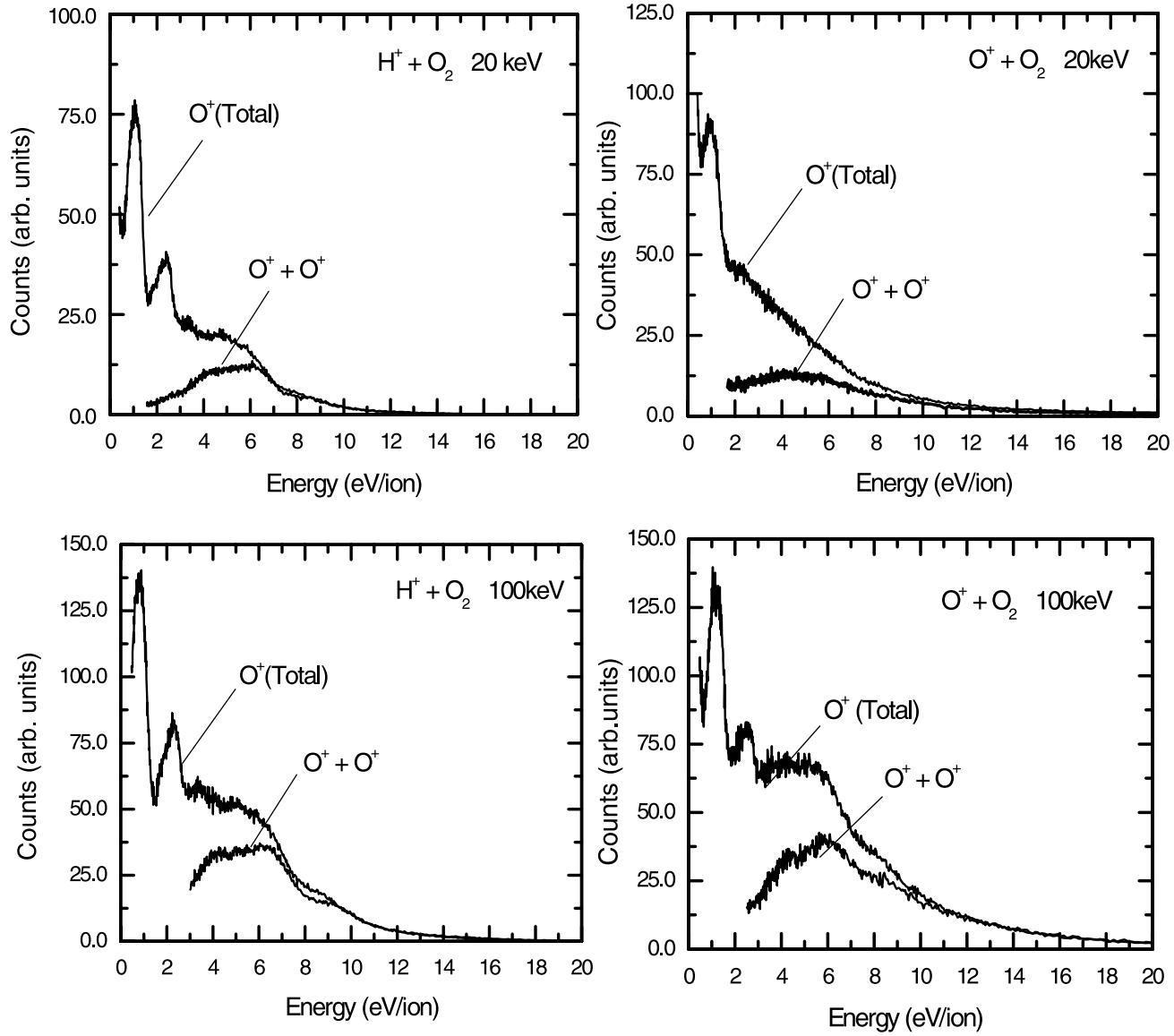

FIG. 4.—Energy distributions of O^+ fragment products emitted at 90° during collisions of H^+ and O^+ incident ions on O_2. Curves labeled $O^+ + O^+$ show energy distributions of events leading to ion pairs, and curves labeled O^+ show energy distributions of all events leading to O^+ production. Contributions from both capture and ionization processes are included. The arbitrary units are the same for each spectrum.

It should also be noted that all our measured energy spectra are Doppler-free as a consequence of our use of the crossed beam arrangement. As our observations are made at 90° to the well-defined target beam, negligible thermal dispersion is introduced into the measured energy spectra.

The present KER spectra can be compared with those of Yousif et al. (1987) and Lafosse et al. (2001) involving low-energy He^+ ions. Lafosse et al. (2001) endeavored to detect a majority of the target products by using weak fields to extract the products. Their TOF spectra, as a result, lack the resolution required to identify contributions from individual vibration states. However, they incorporated measurements of the projectile energy loss and consequently were able to provide unambiguous identification of the states of O_2^+ contributing to the energy spectra. Figure 5 shows the presence of peaks at 0.80, 1.72, 2.2, 3.2, 5.0, and 7.2 eV for the $O^+ + O$ production, which bears a striking resemblance to the low-energy (<10 keV) He^+ work. However, the 2.2 and 3.2 eV peaks both appear at slightly lower energies in the earlier work (2.0 and 3.0 eV, respectively). The compilation and analysis of all published electron impact data by Van Zyl & Stephen (1994) also reveals the same energy groups in the KER spectra. These features originate via the production of unstable precursor states of the O_2^{+*} ion excited in the Frank-Condon region. The KER taken up by the O^+ ions can be used to identify the energies of these states in relation to their dissociation limit (see Table 1 of Yousif et al. 1987). From the known potential energy curves for O_2^{+*} we can associate the first five of the above peaks observed in the present work with excitation to the $3\,^2\Pi_u/B\,^2\Sigma_g^-$, $^2\Sigma_u^-$, $c\,^4\Sigma_u$, $c\,^4\Sigma_u$, and $^2\Pi_u$ states of O_2^{+*}, respectively. The origin of the remaining weak peak at 7.2 eV, not seen by previous workers, remains as yet unknown. Since He^+ ions have a potential energy (PE) of 24.6 eV, they can populate the $c\,^4\Sigma_u$ state resonantly through electron capture processes leading to the production of both 2.2 and 3.2 eV fragment ions. However, H^+ ions (PE = 13.6 eV) are not able to populate this state so easily by capture processes, and so for H^+, the state is more likely to be formed, albeit less efficiently, via pure excitation processes. This view is reinforced in Figure 2, which shows that at 100 keV, the ionization cross sections that require transfers of large amounts of energy are larger than

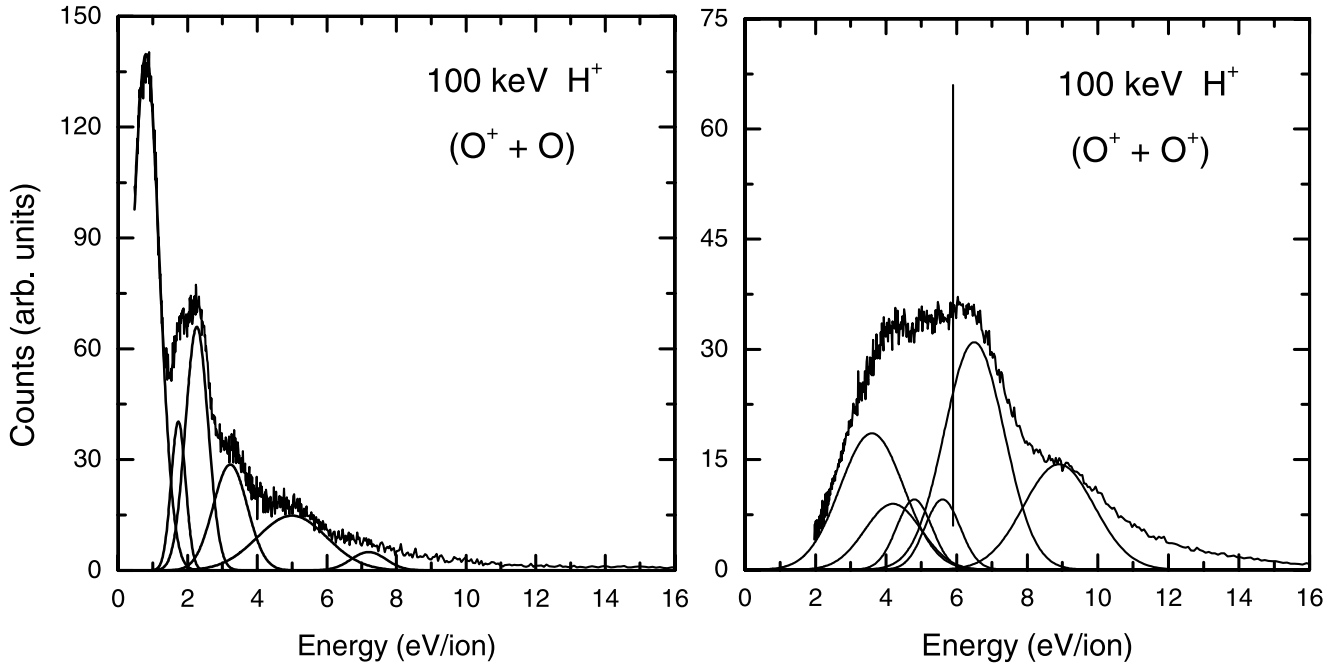

FIG. 5.—Energy distribution of the ion fragments emitted at 90° in collision with 100 keV H^+ (Fig. 3) separated into the $O^+ + O$ and the $O^+ + O^+$ components. Solid curves show Gaussian peaks fitted to the spectra and correspond (see text) to fragmentation arising from known precursor ion states of O_2^{+*} and O_2^{++*}, respectively (Yousif et al. 1987; Lafosse et al. 2001; Lundqvist et al. 1996). The vertical solid line indicates the kinetic energy release expected for a pointlike Coulomb repulsion.

the capture cross sections, for channels leading to similar target products. The population of other states leading to dissociative contributions to nearby peaks can also become probable for H^+, and these may be responsible for pushing the 2.0 and 3.0 eV peaks a little more toward the higher energies.

Fragment ion energy distributions arising from Coulomb explosions, which involve the production of O^+-O^+ ion pairs, also shown in Figure 5, extend over the range 2–14 eV and show substantial structure. It is interesting to note that a Coulomb explosion of the O^+-O^+ system, starting from the equilibrium distance of the neutral O_2 molecule ($r_e = 1.2$ Å), would yield fragment O^+ ions each with an energy of 5.96 eV. Thus, some of the potential energy curves that are being populated in the Frank-Condon region lie above the point charge Coulomb curve for two singly charged particles. These KER spectra can be interpreted with the aid of the definitive *e*-impact, Doppler-free experiments of Lundqvist et al. (1996), who have observed and identified a large number of vibrationally resolved channels. Our Gaussian fittings show the presence of major peaks at the energies of 3.6, 6.5, and 8.9 eV and minor peaks at the energies of 4.2, 4.8, and 5.6 eV. A comparison with the table provided by Lundqvist et al. shows that these features originate via the production of unstable precursor states of the O_2^{++*} ion excited in the Frank-Condon region and correspond to processes involving $W\,^3\Delta_u$, $c\,^3\Pi_u$, and $I\,^5\Sigma_u^-$; and $B\,^3\Sigma_u^-$, $1\,^1\Delta_u$, and $B\,^3\Pi_g\,O_2^{++*}$ ions, respectively. All these ions dissociate to form a pair of $O^+(^4S)$ and $O^+(^2D)$ ions with the exception of $B\,^3\Pi_g$, which gives rise to a pair of two $O^+(^4S)$ ions. It should be noted, however, that there are enormous quantitative differences between the *e*-impact work and the present fast ion results. For example, the major channel, by over a factor of 2 in the *e*-impact work, involves the $B\,^3\Pi_g\,O_2^{++}$ ion, which is only seen as a very minor channel in the present work. On the other hand, the $W\,^3\Delta_u$ channel makes a much larger contribution in the fast ion work.

Fragment ion kinetic energy release distributions of all O^+ ions ($O^+ + O$ and the $O^+ + O^+$ ion pairs) formed in the dissociative ionization of O_2 by 1 MeV H^+ and O^+ ions have been measured by Steuer et al. (1977). Their findings show the presence of a number of energy groups that are in agreement with the present work and the data involving other projectiles, including protons. Clearly, at sufficiently high velocities and low projectile charge, the fragmentation process is not greatly influenced by the presence of the passing projectiles, and, as the characteristic fragmentation times ($\approx$10 fs) are larger than the collision times, the KER spectra are dictated mainly by the molecular states excited during the collisions. However, the 1 MeV data do show that O^+ projectiles, in contrast to H^+ ions of the same energy, give rise to a significant fraction of O^+ fragment ions with energies $\geq$10 eV—a feature that is also apparent in the present data at 100 keV (Fig. 5). Furthermore, the observation of a peak at around 9.0 eV in their O^+ spectra at 1 MeV indicates the increasing importance of the Coulomb explosion process (see Fig. 5).

For a complete modeling of the Jovian magnetosphere, measurements for H^+ and O^+ projectiles below 10 keV and above 100 keV are also needed. Rudd et al. (1983) have measured cross sections for total electron production from ionization of O_2 by 5–4000 keV H^+ ions as well as that for electron capture up to 150 keV. These data are generally considered to be highly reliable and are compared to our measurements in Figure 6. The capture data of Rudd et al. are derived from subtracting their electron production cross sections from their cross sections for the production of total positive target ion charge and consequently correspond to our cross sections for the sum of the channels (1), (2), (3), and (4). For clarity, capture cross sections and cross sections for the total positive ion charge are shown only. Also included in Figure 6 are the compilation cross sections of Rees (1989) extending from 40 eV to 240 keV and of Basu et al. (1987) extending over the 1–1000 keV

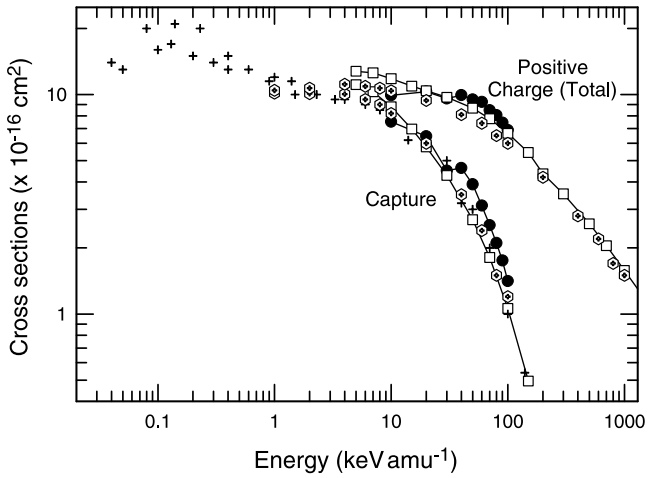

FIG. 6.—Comparison of our total one-electron-capture cross sections (channels [1] + [2] + [3] + [4]) and our total positive ion charge production cross sections (channels [1] + [2] + 2×[3] + 2×[4] + [5] + [6] + 2×[7]) with a compilation of previous measurements over a large energy range. *Capture: Triangles*, present data; *open squares*, Rudd et al. (1983); *plus signs*, Rees (1989); *open hexagons*, Basu et al. (1987). *Total positive charge: Filled triangles*, present data; *squares with center dots*, Rudd et al. (1983); *hexagons with center dots*, Basu et al. (1987).

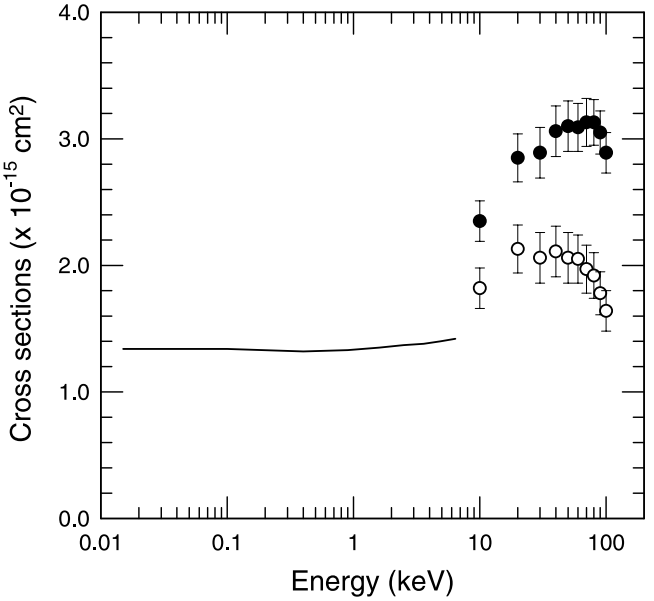

FIG. 7.—Cross sections for the production of positive ion charge in collision of O^+ with O_2 compared with previous measurements. *Filled circles,* present data for total positive ion charge production (channels [1] + [2] + 2×[3] + 2×[4] + [5] + [6] +2×[7]); *solid line,* Stebbings et al. (1963b) data; *open circles,* present data for net positive ion charge production (channels [1] + [2] + [3] + [4]).

energy range. As seen, the overall agreement between the three sets of data is very good and is well within the combined uncertainty.

For O^+ impact, the cross sections of Stebbings et al. (1963b) for the production of total positive target ion charge over the energy range 15–5000 eV are compared to our measurements in Figure 7. As is evident, the Stebbings et al. cross sections are almost a factor of 2 smaller than ours. The reason for such a large discrepancy is not obvious, as we both use the H^+ one-electron-capture cross sections of Stier & Barnett (1956) to normalize our data. However, a possible answer may lie in the measuring procedure adopted by Stebbings et al. They crossed their O^+ projectiles with a thermal energy beam of O_2 at right angles and surrounded the interaction region with a negatively biased cylindrical collector along the O^+ beam axis held at a "few volts" (see Stebbings et al. 1963a for details) to collect the positive current of the target ions formed within the interaction region. The cylindrical collector geometry was used to ensure that projectiles moving along the cylindrical axis remained unperturbed by the collection field even at very low collision energies. Because of the use of this arrangement, it is conceivable that electrons produced by collisions may not be rejected completely by the very weak field present inside the cylinder, where the majority of the collisions are likely to occur. Insufficient suppression of electrons would result in the lowering of the positive current measured. Figure 2 shows that for O^+, channels (3)–(7) leading to electron production are not insignificant even at our lowest energy of 10 keV. If we were to assume that electron repulsion was not adequate in the Stebbings et al. experiment, then their measured positive current would correspond to a net positive current from the channels (1), (2), (3), and (4). We include our measurements for this sum in Figure 7 as open circles. As seen, this set of cross sections is much closer in magnitude to the Stebbings et al. cross sections. In addition, the escape of energetic O^+ target fragments from the collector ends would further lower the positive current measured. Figure 4 reveals that the majority of the fragment ions fly away with energies well in excess of 1 eV. Consequently, the biasing of a "few volts" will be insufficient to suppress escape of these energetic fragments from the collector ends. This combined influence of insufficient electron suppression and energetic fragment escape may well be responsible for the large discrepancy seen between our measurements and those of Stebbings et al. The disagreement would be greatest at the highest energies of Stebbings et al. but would decrease substantially at their very low energies, as the ionization cross sections become insignificant at these energies, as would those for channels leading to fragmentation. We therefore consider that the results of Stebbings et al. represent mainly the nondissociative charge exchange channel (1).

3.3. *Charge Exchange and Ionization in Europa's Oxygen Atmosphere*

Since Europa orbits within Jupiter's giant magnetosphere, it experiences a relatively intense flux of energetic ions and electrons (Cooper et al. 2001; Paranicas et al. 2002). These energetic particles not only sputter the icy surface, but they also cause chemical change, a process called radiolysis (Johnson et al. 2003, 2004). A primary product of the radiolysis of ice is its decomposition into molecular hydrogen and oxygen. Whereas the hydrogen molecules readily escape from Europa's gravitational field, the heavier oxygen molecules do not. Since the molecular oxygen does not stick to the surface at Europa's surface temperatures, a thin oxygen atmosphere accumulates. The oxygen density of the atmosphere builds up until the supply by radiolysis is in a steady state with atmospheric loss processes (Johnson et al. 1982; Saur et al. 1998; Shematovich & Johnson 2001; Shematovich et al. 2005). Loss of Europa's atmosphere is due primarily to its interaction with the plasma ions and electrons trapped in Jupiter's magnetosphere.

The hydrogen molecules that directly escape and the oxygen atoms and molecules that are removed collisionally from Europa's atmosphere orbit Jupiter until they are dissociated or ionized. Therefore, the ejected hydrogen and oxygen, and their neutral dissociation products, form an extended neutral

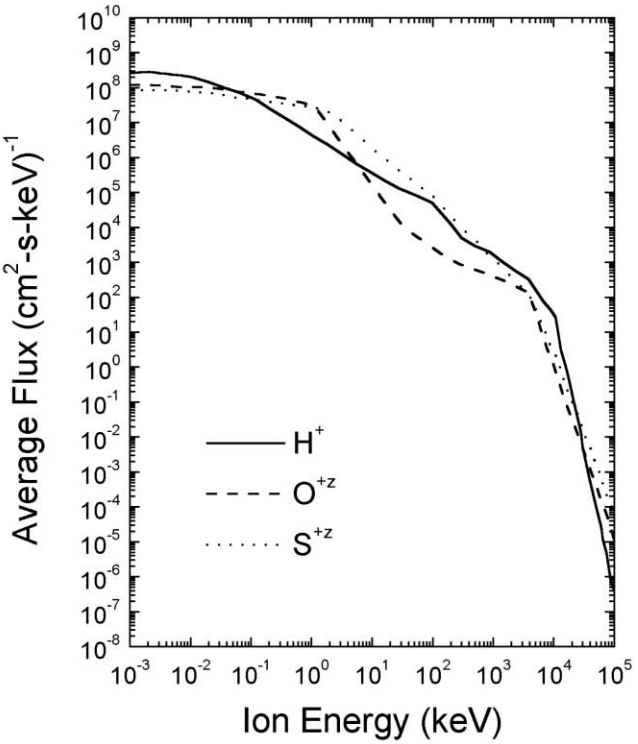

FIG. 8.—Average particle flux upstream of Europa for H^+, O^{+z}, and S^{+z} (J. Cooper 2004, private communication); this flux is variable, and the average z is close to 1 for oxygen, but comparable amounts of singly ionized and doubly ionized sulfur are present.

atmosphere (Burger & Johnson 2004). If the lifetimes are long enough, components of this cloud can form a toroidal neutral atmosphere gravitationally bound to Jupiter and centered at Europa's orbital radius (Schreier et al. 1993). Recently, Europa's extended neutral atmosphere was observed, both directly and indirectly, by instruments on board *Cassini* (Hansen et al. 2003; Mauk et al. 2003) and *Galileo* (Lagg et al. 2003).

Here we focus on the molecular oxygen component of Europa's atmosphere. This consists of oxygen gravitationally bound to Europa and an extended molecular oxygen atmosphere that orbits with Europa but is gravitationally bound to Jupiter. The extended molecular oxygen cloud has a content projected onto Europa's surface of the order of 10^{14} O_2 cm^{-2}. It extends continuously down into Europa's thin gravitationally bound oxygen atmosphere, which has a column density of $\sim 10^{15}$ O_2 cm^{-2} (Shematovich et al. 2005). Although these atmospheres are extremely rarefied and form an ambient gas rather than a normal atmosphere, they are important indicators of the processing of Europa's surface. These atmospheres are also penetrated by the energetic ions trapped in Jupiter's magnetic field. The incident fluxes are shown in Figure 8. The thin atmosphere bound to Europa also has an ionosphere observed by *Galileo* (Kliore et al. 1997). Unlike at the Earth, the principal source of ionization is due to the Jupiter's magnetospheric plasma (Bagenal 1994), in which Europa orbits. Although the plasma electrons might be the primary ionization source, the interaction of Jupiter's fields and trapped plasma with Europa's atmosphere and ionosphere is complex. The plasma electrons roughly follow the field lines, which are highly distorted near Europa. This can significantly reduce their energies and the incident electron flux (Saur et al. 1998). The energetic ions, however, exhibit gyromotion about the field lines with gyroradii comparable to Europa's radius (Johnson 1990; Cooper et al. 2001). Therefore, they can have access to both the atmosphere and surface.

TABLE 3
O_2 CHARGE EXCHANGE AND ION PRODUCTION RATES AT EUROPA

O_2 Processes[a]	Rates (10^{-8} s^{-1})
H^+ charge exchange (1)–(4)	4.1[b]
O^+ charge exchange (1)–(4)	>0.2[c]
H^+ net ion production (1)–(7)	~5.4
O^+ net ion production (1)–(7)	>0.3[c]
Photoionization	2.8[d]
Electron impact[e] ionization	≤180[f]

[a] Numbers in parentheses indicate processes in channels (1)–(7).
[b] Combined with Rudd et al. (1983) and Basu et al. (1987) data to obtain cross sections over the full energy range for protons in Fig. 8.
[c] Lower limits obtained using only the energy range studied here, 0.01–0.1 MeV, which have uncertainties of the order of 50%. These estimates do not include the sulfur ion contribution to the flux shown in Fig. 8.
[d] Photoabsorption from Shematovich et al. (2005) calculated at the mean solar activity level of $F_{10.7} = 144$ photons cm^{-2} s^{-1}; this varies by about a factor of 2.5 in going from low to high solar activity.
[e] Assumes that the magnetospheric electron flux is unattenuated and undeflected, which is not likely. Therefore, depending on the induced fields, this effect can be 1 or 2 orders of magnitude smaller near Europa's surface (Saur et al. 1998).
[f] Electron impact O_2 ionization (Shematovich et al. 2005); used Bagenal (1994) model of the magnetospheric plasma.

Since the total charge exchange cross sections measured here exceed 10^{-15} cm^2 and the atmospheric column is $\sim 10^{15}$ O_2 cm^{-2}, as discussed above, the energetic O^+ ions that penetrate the gravitationally bound oxygen atmosphere will mostly be neutralized by charge exchange processes. They are then unaffected by the local fields. Depending on their direction of motion, they can impact the surface, causing sputtering, or they can escape the system. Therefore, two critical issues are affected by the cross sections measured here. The first is the contribution of the energetic protons and oxygen ions to the ionization and dissociation rates of Europa's oxygen atmosphere. The second is the production of energetic neutrals by charge exchange, since detection of these neutrals will be used to image the oxygen atmosphere in a future mission.

In Table 3 we give the ion production rates by the various processes acting at Europa. For the energetic protons, we use our data with that of Rudd et al. (1983), Basu et al. (1987), and Rees (1989) in Figure 6 to obtain the total charge exchange and ion production cross sections times the ion flux over the full range of energies in Figure 8. For the incident O^+ component, we obtain a lower limit using only the measurements made here for 10–100 keV ions times the ion fluxes in Figure 8. It is seen that the net ion production rate produced by the energetic ions is larger than that produced by UV photons. However, it is smaller than the upper limit estimate given for incident plasma electrons. The latter is based on the ambient conditions downstream of Europa. In the extended neutral cloud this is a good approximation, and therefore the plasma electrons are likely the dominant source of ionization in that region. However, as these electrons flow through the neutral cloud, enter the interaction region, and penetrate the atmosphere, they cool by collisions and are deflected by the local fields. Therefore, depending on the nature of this interaction, ionization by the energetic ions can become the dominant ion production process in regions of Europa's atmosphere.

Because a significant fraction of the O_2 dissociation products can have energies greater than the escape energy (~0.34 eV),

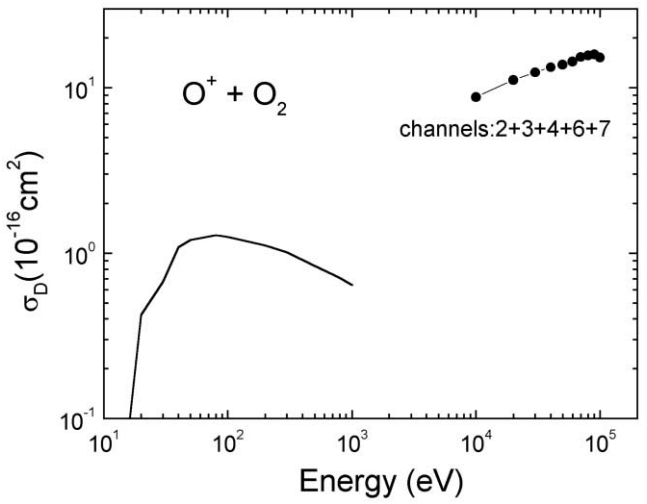

FIG. 9.—Dissociation of molecular oxygen by incident oxygen ions. *Solid line:* Calculation from Johnson et al. (2002). *Dots:* Sum of results from channels (2), (3), (4), (6), and (7). These are each lower bounds to the total dissociation cross sections for incident O^+ ions over the energy region for which they are given.

dissociation by the incident electrons and photons is an important atmospheric loss mechanism for oxygen ions and atoms (Saur et al. 1998; Shematovich et al. 2005). Since momentum conservation requires that the O atoms from O_2 (channels [2], [4], [6], and [7]) have the same fragment energy distribution as the partner O^+ fragment ions, the distributions in Figure 4 also apply to the O fragments.

Although the energetic (>10 keV) component of ions is the predominant carrier of energy in the trapped Jovian plasma, a larger flux of lower energy protons and oxygen and sulfur ions is seen to also flow onto Europa's atmosphere, as shown in Figure 8 (Bagenal 1994; J. Cooper 2004, private communication). Unlike the fast ions, these lower energy ions produce dissociation by direct knock-on collisions, which are described by the so-called momentum transfer cross sections (e.g., Johnson 1982). Such collisions will have a very different spectrum of ejected O energies (Johnson et al. 2002). In Figure 9 we show the net dissociation cross section found here for $O^+ + O_2$ (channels [2], [3], [4], [6], and [7]). This is a lower limit to the total electronically induced dissociation cross sections that involve excitation of electrons into high-lying repulsive energy states. These cross sections are compared in Figure 9 to the dissociation cross section calculated for knock-on collisions by an incident oxygen ion (Johnson et al. 2002). The dependence of the measured cross section on energy above 10 keV in Figure 9 and the product energies in Figure 5 indicate that dissociation in response to electronic excitations by fast ions is efficient. Integrating the two curves over the O^+ flux in Figure 8, the net contributions to dissociation are comparable. Roughly extrapolating the results for <100 keV down to the solid curve, one finds that the net dissociation rate by the incident O^+ ($\sim 1.5 \times 10^{-8}$ s^{-1}) is more than 3 times that for the momentum transfer collisions only. Including the proton flux, which has a very small momentum transfer contribution, increases the importance of electronically induced dissociation processes. Therefore, electronic contributions to dissociation by incident ions must be included in modeling the interaction of the ion flux in Figure 8 with the satellite atmospheres, and the momentum transfer collisional dissociation rates used to model Europa's atmospheric loss (Saur et al. 1998; Shematovich et al. 2005) are lower limits to the total ion-induced dissociation rates.

Finally, the energetic protons and oxygen ions have rather large charge exchange cross sections. The energetic neutrals formed by this process disconnect from the field lines. A fraction will directly impact Europa's surface, as discussed, but the remainder will exit in all directions. Since the escape energy from Jupiter's system is $\sim$18 eV amu^{-1}, the neutralized ions not only escape from Europa, but they also escape from Jupiter, populating the solar system, as observed for the sodium from Io (Mendillo et al. 1990). Since these energetic neutrals can be readily detected by an orbiting spacecraft and they move on relatively straight trajectories, they can be used to image Europa's atmosphere. Using such an instrument on *Cassini*, Mauk et al. (2003) initially thought they observed the charge-exchanged neutrals from the oxygen cloud. They in fact imaged Europa's extended hydrogen cloud (Shematovich et al. 2005; Hansen et al. 2003). However, a number of instruments have been proposed for a new spacecraft (*JIMO*, *Jupiter's Icy Moon Orbiter*) that will use charge exchange neutrals to image Europa's thin atmosphere. Assuming roughly isotropic flow onto the atmosphere by the fast (>10 keV) ions, the net flux of energetic neutrals (10–100 keV) is $\sim 10^7$ neutrals cm^{-2} s^{-1} sr^{-1} from Europa's atmosphere. In addition, an instrument that detects dissociation products (>1 eV) by negative ion formation has been proposed. Based on the results in Figures 3 and 4, a significant fraction of the atmosphere dissociation products will have sufficient energies to be detected, allowing one to directly image the dissociation events occurring in Europa's atmosphere.

4. CONCLUSIONS

Measurements of the cross sections for charge exchange and ionization of O_2 by 10–100 keV protons and oxygen ions were carried out. The ions in this energy range carry a large fraction of the plasma ion energy in the Jovian magnetosphere. In addition, the dissociative and nondissociative channels were separately measured, as were the energies of the dissociation products. The total cross sections obtained here were consistent with those measured by others (Rudd et al. 1983; Basu et al. 1987). However, the results for incident O^+ disagree with the total positive ion production cross sections of Stebbings et al. (1963a, 1963b). Because we were able to separate the dissociation channels, which are significant for incident O^+, and measure the fragments' energies, we have shown that Stebbings et al. most probably measured the electron capture processes (channels [1] and [2]) only. A comparison of the total dissociation cross sections for fast ions with those calculated at lower energies for incident oxygen atoms or ions in Figure 9 suggested that the electronically induced dissociation processes dominate over the momentum transfer–induced dissociation. Therefore, the estimated atmospheric loss rates at Europa currently based on momentum transfer cross sections must be increased.

Measurements of the fragment dissociation energies were also made. These were compared to the fragment dissociation energies produced by incident electrons and He^+. In all cases the fragment spectrum is dominated by electronic excitation to unstable excited states of O_2^+. For this diatomic molecule, the measured energy spectra also apply to the exiting neutral.

The results here are of interest in understanding the formation and stability of the thin molecular oxygen atmospheres on the icy Galilean satellites (Johnson et al. 2004) and may also be relevant in describing the molecular oxygen content of Saturn's toroidal atmosphere (Young et al. 2005). The atmospheres of Europa and Ganymede are formed by the energetic particle radiation trapped in the Jovian magnetosphere and are also removed by this radiation (e.g., McGrath et al. 2004). The ion production rates at

Europa by the incident energetic ions studied here were shown to be larger than the photoionization rates. These rates can dominate in those regions in which the electron flow into the atmosphere is limited by the induced currents and the distorted local fields. Since a principal loss channel for Europa's atmosphere is that due to charge exchange and dissociation by ion impact, the data presented here are now available for further modeling. In addition, the energetic neutral flux produced by charge exchange will eventually be used to interpret measurements of energetic neutrals used to image these thin oxygen atmospheres.

The authors would like to thank the Brazilian Conselho Nacional de Desenvolvimento Científico e Tecnológico (CNPq) agency for providing funds to H. Luna for a one-year postdoctoral visit to Belfast. M. B. S. and C. J. L. would like to acknowledge support from the UK Engineering and Physical Science Research Council. E. C. M. thanks the International Research Centre for Experimental Physics, Queen's University Belfast, for providing funds for the collaboration. R. E. J. and M. L. would like to acknowledge the support of the Planetary Atmospheres Program of NASA.

REFERENCES

Afrosimov, V. V., Leiko, G. A., Mamaev, Yu. A., Panov, M. N., & Vuiovich, M. 1974, Sov. Phys.—JETP, 38, 243
Auerbach, D. J. 1988, in Atomic and Molecular Beam Methods, Vol. 1, ed. G. Scoles (Oxford: Oxford Univ. Press), 365
Bagenal, F. 1994, J. Geophys. Res., 99, 11043
Basu, B., Jasperse, J. R., Robinson, R. M., Vondrak, R. R., & Evans, D. S. 1987, J. Geophys. Res., 92, 5920
Browning, R., & Gilbody, H. B. 1968, J. Phys. B, 1, 1149
Burger, M. H., & Johnson, R. E. 2004, Icarus, 171, 557
Cooper, J. F., Johnson, R. E., Mauk, B. H., Garrett, H. B., & Gehrels, N. 2001, Icarus, 149, 133
Hansen, C. J., Shemansky, D. E., & Hendrix, A. R. 2003, BAAS, 34, 1703
Johnson, R. E. 1982, An Introduction to Atomic and Molecular Collisions (New York: Plenum)
———. 1990, Energetic Charged Particle Interactions with Atmospheres and Surfaces (Berlin: Springer)
Johnson, R. E., Carlson, R. W., Cooper, J. F., Paranicas, C., Moore, M. H., & Wong, M. C. 2004, in Jupiter—The Planet, Satellites and Magnetosphere, ed. F. Bagenal, T. Dowling, & W. B. McKinnon (Cambridge: Cambridge Univ. Press), 485
Johnson, R. E., Lanzerotti, L. J., & Brown, W. L. 1982, Nucl. Instrum. Methods 198, 147
Johnson, R. E., Liu, M., & Tully, C. 2002, Planet. Space Sci., 50, 123
Johnson, R. E., Quickenden, T. I., Cooper, P. D., McKinley, A. J., & Freeman, C. 2003, Astrobiology, 3, 823
Jorgensen, T., Kuyatt, C. E., Lang, W. W., Lorents, D. C., & Sautter, C. A. 1965, Phys. Rev. A, 140, 1481
Jurac, S., McGrath, M. A., Johnson, R. E., Richardson, J. D., Vasyliûnas, V. M., & Eviatar, A. 2002, Geophys. Res. Lett., 29(24), 25
Kliore, A. J., Hinson, D. P., Fraser, F. M., Nagy, A. F., & Cravens, T. E. 1997, Science, 277, 355
Krimigis, S. M., et al. 2005, Science, 307, 1270
Lafosse, A., Houver, J. C., & Dowek, D. 2001, J. Phys. B, 34, 819
Lagg, A., Krupp, N., Woch, J., & Williams, D. 2003, Geophys. Res. Lett., 30(11), 10
Lindsay, B. G., Merrill, R. L., Straub, H. C., Smith, K. A., & Stebbings, R. F. 1998, Phys. Rev. A, 57, 331
Luna, H., Michael, M., Shah, M. B., Johnson, R. E., Latimer, C. J., & McConkey, J. W. 2003, J. Geophys. Res., 108(E4), 14
Lundqvist, M., Edvardsson, D., Baltzer, P., Larsson, M., & Wannberg, B. 1996, J. Phys. B, 29, 499
Mauk, B. H., Mitchell, D. G., Krimigis, S. M., Roelof, E. C., & Paranicas, C. P. 2003, Nature, 421, 920
McCartney, P. C. E., McGrath, C., McConkey, J. W., Shah, M. B., & Geddes, J. 1999, J. Phys. B, 32, 5103
McGrath, C., Shah, M. B., McCartney, P. C. E., & McConkey, J. W. 2001, Phys. Rev. A, 64, 062712
McGrath, M. A., Lellouch, E., Strobel, D. F., Feldman, P. D., & Johnson, R. E. 2004, in Jupiter-The Planet, Satellites and Magnetosphere, ed. F. Bagenal, T. Dowling, & W. B. McKinnon (Cambridge: Cambridge Univ. Press), 457
Mendillo, M., Baumgardner, J., Flynn, B., & Hughes, W. J. 1990, Nature, 348, 312
Paranicas, C., Mauk, B. H., Ratliff, J. M., Cohen, C., & Johnson, R. E. 2002, Geophys. Res. Lett., 29(5), 18
Rees, M. H. 1989, Physics and Chemistry of the Upper Atmosphere (Cambridge: Cambridge Univ. Press)
Rudd, M. E., DuBois, R. D., Toburen, L. H., Ratcliffe, C. A., & Goffe, T. V. 1983, Phys. Rev. A, 28, 3244
Saur, J., Strobel, D. F., & Neubauer, F. M. 1998, J. Geophys. Res., 103, 19947
Schreier, R., Eviatar, A., Vasiliunas, V. M., & Richardson, J. D. 1993, J. Geophys. Res., 98, 21231
Shematovich, V. I., & Johnson, R. E. 2001, Adv. Space Res., 27, 1881
Shematovich, V. I., Johnson, R. E., Cooper, J. H., & Wong, M. 2005, Icarus, 173, 480
Stebbings, R. F., Smith, A. C., & Gilbody, H. B. 1963a, J. Chem. Phys., 38, 2280
Stebbings, R. F., Turner, B. R., & Rutherford, J. A. 1966, J. Geophys. Res., 71, 771
Stebbings, R. F., Turner, B. R., & Smith, A. C. 1963b, J. Chem. Phys., 38, 2277
Steuer, M. F., Wood, R. M., & Edwards, A. K. 1977, Phys. Rev. A, 16, 1873
Stier, P. M., & Barnett, C. F. 1956, Phys. Rev., 103, 896
Van Zyl, B., & Stephen, T. M. 1994, Phys. Rev. A, 50, 3164
Young, D. T., et al. 2005, Science, 307, 1262
Yousif, F. B., Lindsay, B. G., Simpson, F. R., & Latimer, C. J. 1987, J. Phys. B, 20, 5079